

Future changes in propagating and non-propagating diurnal rainfall over East Asia

Wan-Ru Huang¹  · S.-Y. Simon Wang^{2,3}

Received: 1 January 2016 / Accepted: 7 September 2016 / Published online: 19 September 2016
© The Author(s) 2016. This article is published with open access at Springerlink.com

Abstract The characteristics of diurnal rainfall in the East Asian continent consist of a propagating regime over the Yangtze River and a non-propagating regime in southeast China. Simulations of these two diurnal rainfall regimes by 18 CMIP5 models were evaluated from the historical experiment of 1981–2005. The evaluation led to the identification of one model, the CMCC-CM that replicated the key characteristics of diurnal rainfall regimes including the propagation of moisture convergence. Using the CMCC-CM to assess the future (2076–2100) change of diurnal evolution and propagation projected by the RCP4.5 experiment, it was found that propagating diurnal rainfall will enhance and expand southward into the non-propagating regime in southeast China. This change in diurnal rainfall is attributed to the intensification of diurnal land–sea thermal contrast over eastern China and the southward shift of the upper-level jet stream over 20°–30°N. Similar projected changes in diurnal rainfall and associated large-scale dynamical mechanisms were also depicted by four other models (GFDL-ESM2G, GFDL-ESM2M, MRI-CGCM3, and MRI-ESM1) showing a higher skill in representing the diurnal rainfall regimes over East Asia. If such model

projection holds true, southeast China will experience an increase in the eastward propagating diurnal rainfall, which could further impact Taiwan.

Keywords Diurnal rainfall · CMIP5 · East Asia · RCP4.5

1 Introduction

Simulation of diurnal rainfall cycle is one of the greatest challenges facing global climate models (GCMs) (Slingo et al. 2004; Dai and Trenberth 2004). Poor representation of the diurnal cycle affects a model's ability in capturing regional climate variability (Wang et al. 2007; Yuan 2013). Evaluating and improving the simulation of diurnal rainfall (i.e. test from model resolution, convective scheme, radiative scheme, cloud processes, etc.) has been a subject of active research (Lin et al. 2000; Yang and Slingo 2001; Zhang 2003; Collier and Bowman 2004; Dai 2006; Lee et al. 2007; Sato et al. 2009; Li et al. 2015). Earlier studies noted that most GCMs tended to produce inaccurate timing in the evolution of diurnal rainfall, particularly over landmass in which rainfall occurs too early (e.g., Dai 2006; Hara et al. 2009; Yuan et al. 2013). The distribution of diurnal rainfall in GCMs is generally too homogenous (e.g., Collier and Bowman 2004). Furthermore, GCMs tended to misrepresent the propagating behavior of diurnal rainfall in the eastern slope of large mountains (Lee et al. 2007; Ploshay and Lau 2010; Yuan et al. 2012). Increasing model resolution and adjusting treatment of convection are among the common methods in improving diurnal rainfall simulations (e.g., Arakawa and Kitoh 2005; Dirmeyer et al. 2011; Bacmeister et al. 2013; Yuan et al. 2013; Li et al. 2015).

In the East Asian continent, the complex local circulations involving land–sea breezes and mountain–valley

Electronic supplementary material The online version of this article (doi:10.1007/s00382-016-3348-4) contains supplementary material, which is available to authorized users.

✉ Wan-Ru Huang
wrhuang@ntnu.edu.tw

- ¹ Department of Earth Sciences, National Taiwan Normal University, No. 88, Sec. 4, Tingchou Rd., Wenshan District, Taipei 11677, Taiwan, ROC
- ² Utah Climate Center, Utah State University, Logan, UT, USA
- ³ Department of Plants, Soils, and Climate, Utah State University, Logan, UT, USA

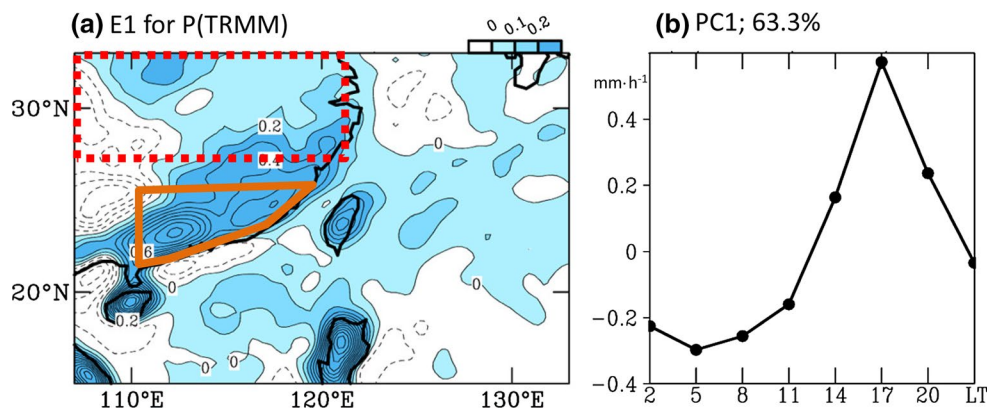


Fig. 1 The first mode of EOF analysis on the long-term, 3-hourly TRMM 3B42 precipitation, following Huang and Chen (2015): **a** eigen-vector (E1) and **b** eigen-coefficient (PC1). In **a**, the domains of the Yangtze River regime (red dotted box) and southeast China regime (orange outline) are marked to help the discussions in the

manuscript. In **b**, the result is presented for southeast China local time (LT), and the % value indicates the percentage of the total variance of the analyzed variable explained by its corresponding EOF mode. The contour interval of **a** is 0.1 and the color scale is given in the top

winds cause regional differences in diurnal rainfall variations (e.g., Zhao et al. 2005; Yu et al. 2007a, b; Kikuchi and Wang 2008; Zhou et al. 2008; Huang and Chan 2012; Huang et al. 2013; Hsu et al. 2014). Observational studies have noted that diurnal rainfall occurring west of 110°E peaks in the midnight or early morning (Asai et al. 1998; Wang et al. 2004; Yu et al. 2007a, b; Li et al. 2008). In the southern part of East Asia to the east of 110°E, the timing of diurnal rainfall over land is dominated by daytime maxima (Yu et al. 2007a, b; Chen et al. 2009). Among these geographical differences, two distinct regimes of diurnal rainfall are present: (a) the Yangtze River (dotted box in Fig. 1) that exhibits a propagating behavior of diurnal rainfall (e.g., Yu et al. 2007a, b) and (b) southeast China (orange outline in Fig. 1) that features non-propagating (afternoon) diurnal rainfall (e.g., Huang et al. 2010). The mechanisms responsible to such a regional difference in diurnal rainfall have been studied extensively (e.g., Wallace 1975; Oki and Musiak 1994; Yang and Slingo 2001; Nesbitt and Zipser 2003; Sorooshian et al. 2002; Yu et al. 2007a, b; Huang et al. 2010; Huang and Wang 2014).

Earlier studies indicated that the solenoidal circulation between the Tibetan Plateau and its leeside lowlands contributes to the extent of the propagating diurnal rainfall over the Yangtze River (Wang et al. 2004; Hirose and Nakamura 2005; Wang et al. 2005; Huang et al. 2010). There, the East Asian jet stream drives the diurnal convection initiated east of the Tibetan Plateau to propagate eastward (Wang et al. 2004). In contrast, the afternoon rainfall peak over the southeast China is mainly induced by the diurnal variation of low-level atmospheric instability associated with solar heating (Huang and Chan 2012). Meanwhile, the afternoon sea breeze over the mountains in southern China results in

low-level convergence of water vapor fluxes to support the formation of afternoon convection (e.g., Yu et al. 2009).

These documented characteristics of diurnal rainfall over East Asia have been used as metrics in evaluating climate models (e.g., Betts and Jakob 2002; Dai and Trenberth 2004). Yuan (2013) evaluated 8 IPCC AR5 models forced by prescribed sea surface temperature over subtropical China by dividing total precipitation into stratiform and convective categories. Yuan (2013) found that most models simulated the stratiform rainfall with a correct diurnal phase but produced the wrong phase for the convective rainfall. In Yuan et al. (2013), one particular model (CAM5) was identified to have the same bias in the convective rainfall in eastern China. To the authors' knowledge, coupled model simulations of the propagating and non-propagating diurnal rainfall regimes over East Asia have not been examined in detail. This aspect of model evaluation is important when it comes to projecting the future diurnal rainfall changes.

As part of the phase-5 Coupled Model Intercomparison Project (CMIP5), several climate modeling centers provide 3-hourly rainfall simulation for both the twentieth century and future climate scenarios (Taylor et al. 2012). The output of these CMIP5 models, which utilize a large variety of horizontal resolution and model physics, gives researchers a new means to evaluate diurnal rainfall simulations and assess projections. The main objective of this study is to evaluate 18 CMIP5 models (listed in Table 1) in the simulation of diurnal rainfall over East Asia. These models and other data sources adopted for the analyses are introduced in Sect. 2. It is anticipated that, among this subset of CMIP5 models, the ones that perform better in resolving diurnal rainfall would provide researchers a better tool to investigate future changes; thus, in Sect. 3 we show that

Table 1 CMIP5 models evaluated and their attributes

Acronym	Model full name	Center/country	Resolution (lon. × lat.)	References
ACCESS1-0	Australian Community Climate and Earth-System Simulator, version 1.0	Commonwealth Scientific and Industrial Research Organization/Bureau of Meteorology, Australia	1.875° × 1.25°	Bi et al. (2013)
ACCESS1-3	Australian Community Climate and Earth-System Simulator, version 1.3	Commonwealth Scientific and Industrial Research Organization/Bureau of Meteorology, Australia	1.875° × 1.25°	Bi et al. (2013)
BCC-CSM1	Beijing Climate Center, Climate System Model, version 1.1	Beijing Climate Center, Meteorological Administration, China	2.8° × 2.8°	Xin et al. (2013)
BCC-CSM1-m	Beijing Climate Center, Climate System Model, version 1.1 (moderate resolution)	Beijing Climate Center, Meteorological Administration, China	1.125° × 1.125°	Xin et al. (2013)
BNU-ESM	Beijing Normal University-Earth System Model	College of Global Change and Earth System Science (GCESS), China	2.8° × 2.8°	Ji et al. (2014)
CMCC-CM	Centro Euro-Mediterraneo sui Cambiamenti Climatici (CCMC) Climate Model	Centro Euro-Mediterraneo sui Cambiamenti Climatici, Italy	0.75° × 0.75°	Scoccimarro et al. (2011)
CNRM-CM5	Centre National de Recherches Météorologiques Coupled Global Climate Model, version 5	National Centre for Meteorological Research, France	1.4° × 1.4°	Volodroire et al. (2013)
GFDL-CM3	Geophysical Fluid Dynamics Laboratory Climate Model version 3	NOAA Geophysical Fluid Dynamics Laboratory, USA	2.5° × 2.0°	Donner et al. (2011)
GFDL-ESM2G	Geophysical Fluid Dynamics Laboratory Earth Science Model 2 with Generalized Ocean Layer Dynamics component	NOAA Geophysical Fluid Dynamics Laboratory, USA	2.5° × 2.0°	Donner et al. (2011)
GFDL-ESM2M	Geophysical Fluid Dynamics Laboratory Earth Science Model 2 with Modular Ocean Model, version 4.1	NOAA Geophysical Fluid Dynamics Laboratory, USA	2.5° × 2.0°	Donner et al. (2011)
INMCM4	Institute of Numerical Mathematics Coupled Model, version 4.0	Institute for Numerical Mathematics, Russia	2.0° × 1.5°	Volodin et al. (2010)
IPSL-CM5A-LR	L'Institut Pierre-Simon Laplace Coupled Model, version 5A, low resolution	Institute Pierre Simon Laplace, France	3.75° × 1.875°	Dufresne et al. (2013)
IPSL-CM5A-MR	L'Institut Pierre-Simon Laplace Coupled Model, version 5A, medium resolution	Institute Pierre Simon Laplace, France	2.5° × 1.25°	Dufresne et al. (2013)
MIROC5	Model for Interdisciplinary Research on Climate, version 5	Atmosphere and Ocean Research Institute (The University of Tokyo), National Institute for Environmental Studies, and Japan Agency for Marine-Earth Science and Technology, Japan	1.4° × 1.4°	Watanabe et al. (2011)
MIROC-ESM	Model for Interdisciplinary Research on Climate Earth System Model	Japan Agency for Marine-Earth Science and Technology, Atmosphere and Ocean Research Institute (The University of Tokyo), and National Institute for Environmental Studies, Japan	2.8° × 2.8°	Watanabe et al. (2011)
MIROC-ESM-CHEM	Model for Interdisciplinary Research on Climate Earth System Model, chemistry coupled version	Japan Agency for Marine-Earth Science and Technology, Atmosphere and Ocean Research Institute (The University of Tokyo), and National Institute for Environmental Studies, Japan	2.8° × 2.8°	Watanabe et al. (2011)

Table 1 continued

Acronym	Model full name	Center/country	Resolution (lon. × lat.)	References
MRI-CGCM3	Meteorological Research Institute Coupled General Circulation Model, version 3	Meteorological Research Institute, Japan	1.1° × 1.1°	Yukimoto et al. (2012)
MRI-ESM1	Meteorological Research Institute—Earth System Model version 1	Meteorological Research Institute, Japan	1.1° × 1.1°	Yukimoto et al. (2012)

one particular model, the Centro Euro-Mediterraneo sui Cambiamenti Climatici Climate Model (hereafter CMCC-CM) (Scoccimarro et al. 2011), was capable of depicting both the correct timing of propagating diurnal rainfall over the Yangtze River and the non-propagating diurnal rainfall over southeast China. In Sect. 4, the characteristics and possible causes of the projected change in the diurnal rainfall over the focused areas are discussed. A conclusion is given in Sect. 5.

2 Data and method

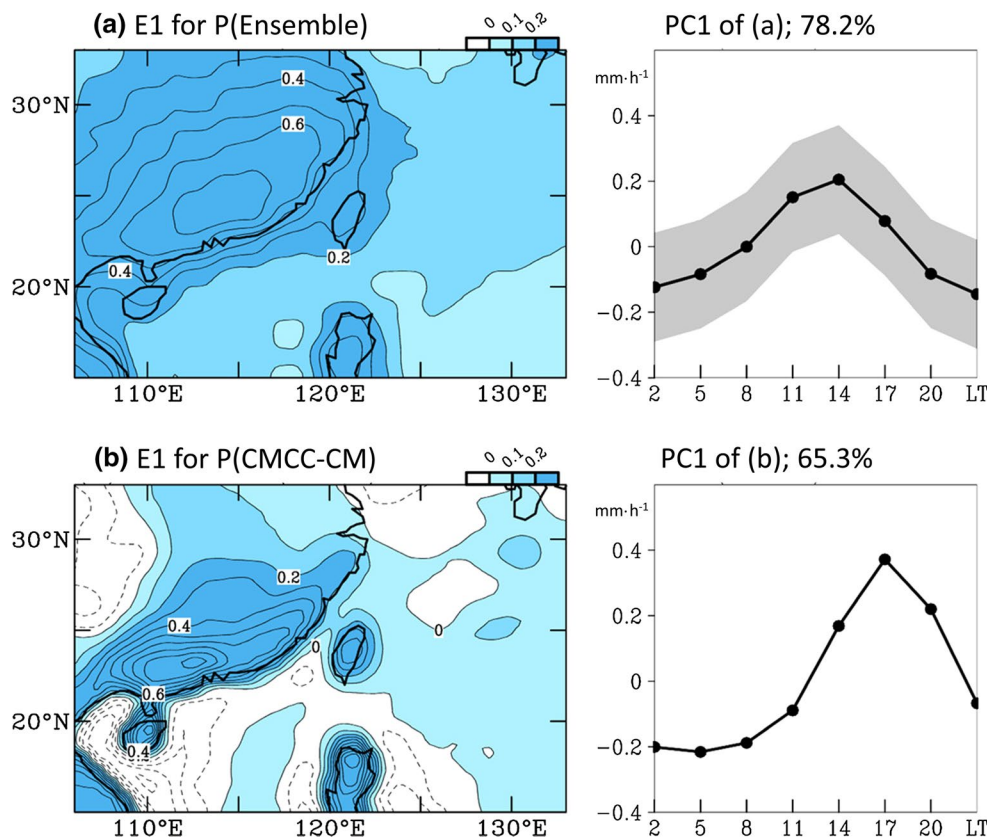
The 18 CMIP5 models that provide 3-hourly rainfall output for both the historical experiment (for the present time period from 1981 to 2005) and the RCP4.5 experiment (for the future period from 2076 to 2100) are listed in Table 1 for their name, institute, horizontal resolution, and references. These model outputs were produced from fully coupled simulations, which are different from those forced by prescribed SST as used in Yuan (2013). One model that stood out from the evaluation (to be discussed in Sect. 3) is the CMCC-CM; it comprises the OPA 8.2 ocean component (Madec et al. 1998) and the ECHAM5 atmospheric component (Roeckner et al. 2006). The parameterization of convection in CMCC-CM uses a modified mass flux concept (Tiedtke 1989), following Nordeng (1994).

For observational data, we used 3-hourly Tropical Rainfall Measuring Mission (TRMM) 3B42 satellite precipitation (Simpson et al. 1996). The TRMM 3B42 dataset provides rain rate beginning in 1998 at the spatial resolution of 0.25° longitude × 0.25° latitude. TRMM has been widely used for the depiction of diurnal rainfall over East Asia (Hong et al. 2005; Zhou et al. 2008; Huang and Chan 2012; Huang and Wang 2014). Other meteorological variables (including wind fields, humidity, etc.) were derived from the 3-hourly Modern-Era Retrospective Analysis for Research and Applications (MERRA) reanalysis (Rienecker et al. 2011) at the spatial resolution of 0.667° longitude × 0.5° latitude. Hereafter, the analyses focus on May and June for the pronounced diurnal rainfall variability and associated eastward propagation (e.g., Wang et al. 2012; Chang et al. 2015). All results are presented for southeast China local time, which is the universal time + 8 h (i.e. 08 LT corresponds to 00 UTC).

3 The simulation of diurnal variation at present climate

The spatial–temporal variations of diurnal rainfall were depicted by the Empirical Orthogonal Function (EOF) analysis applied on the long-term, 3-hourly TRMM

Fig. 2 Similar to Fig. 1, but for the 3-hourly precipitation from: **a** the ensemble mean of 18 CMIP5 models listed in Table 1, **b** the CMCC-CM. In **a**, the spread between the ensemble members are shaded by the grey color. The contour interval of **a, b** is 0.1 and the color scale is given in their top



precipitation, following Huang and Chen (2015). The first EOF (Fig. 1a) portrays the geographical dependence of diurnal rainfall regimes over East Asia, one along the Yangtze River and the other over southeast China. The southeast China regime features non-propagating diurnal rainfall with the maximum occurring around 17 local time (Yu et al. 2007a, b; Chen et al. 2009), while the Yangtze River regime exhibits a propagation with an early morning maximum west of 110°E and an afternoon/evening maximum to the east (Asai et al. 1998; Wang et al. 2004; Yu et al. 2007a, b; Li et al. 2008). The first principal component (PC) in Fig. 1b can be used to infer the temporal characteristics of afternoon rainfall peak over the two regimes. The negative values in PC1 and E1 of Fig. 1b together infer the “early morning rainfall peak” over the upper Yangtze River at 2–11 local time. Combined with the transition depicted by the 2nd EOF between morning and afternoon (shown in the Supplementary Fig. S1a), an eastward propagation of the diurnal rainfall along the Yangtze River is duly delineated. Hence, the EOF analysis was used as a metric to evaluate the general evolution of diurnal rainfall simulations over East Asia.

Following Fig. 1 the EOF analysis of the all-model ensemble mean of diurnal rainfall is shown in Fig. 2a. The ensemble simulations depicted the overall land–sea contrast with a large diurnal variability over land, similar to the

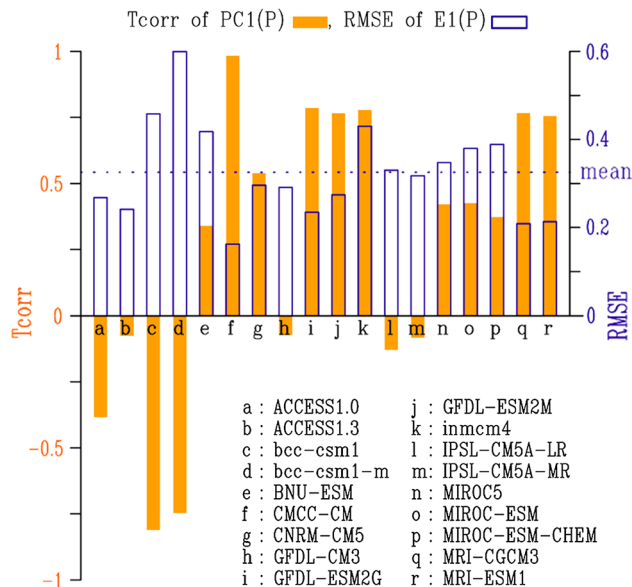


Fig. 3 The evaluation of 18 CMIP5 models’ performance based on the individual EOF results of the diurnal rainfall over the same domain of Fig. 1a. The orange filled bars represent the temporal correlation coefficient (Tcorr) between the first PCs of observed and simulated rainfall. The blue outlined bars represent the spatial root-mean-square-error (RMSE) between the first EOFs of observed and simulated rainfall. The blue dotted line indicates the ensemble mean of the spatial RMSE. The corresponding models of “a” to “r” are listed in the right bottom

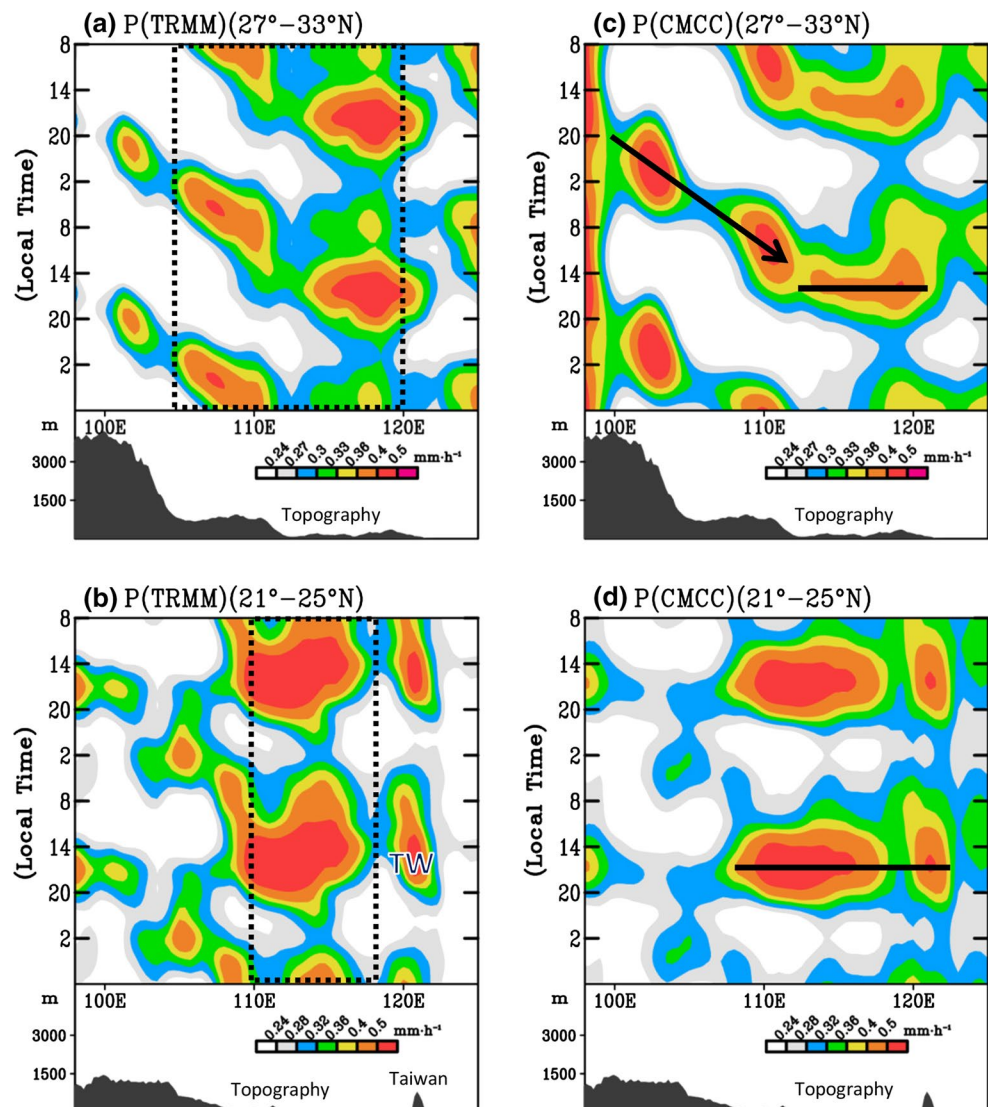
observation. However, the ensemble simulations failed to produce the midnight/early morning rainfall over the Yangtze River west of 110°E, implying a deficiency in capturing the propagation of diurnal rainfall. Moreover, the simulated diurnal rainfall maximum occurs 3–6 h earlier than the observation, as shown in the PC of Fig. 2a. These biases echo those observed by Yuan (2013) that most GCMs could not simulate the correct timing of diurnal rainfall in East Asia.

Next, we evaluated the individual CMIP5 models by conducting the EOF analysis over the domain of Fig. 2a. Based on the individual EOF results (not shown), two variables were compared: (1) the temporal correlation coefficient (Tcorr) between the first PCs of observed and simulated rainfall and (2) the spatial root-mean-square-error (RMSE) between the first EOFs of observed and simulated rainfall. The evaluation of Tcorr and RMSE is shown in Fig. 3. Among the 18 models, CMCC-CM stands out

by exhibiting the highest Tcorr with the lowest RMSE. Although four other models (GFDL-ESM2G, GFDL-ESM2M, MRI-CGCM3, and MRI-ESM1) also appeared to perform better than the rest, their phasing of diurnal rainfall is too early (not shown); a similar problem was noted for MRI-CGCM3 by Yuan (2013). As shown in Fig. 2b, CMCC-CM was able to depict (1) an accurate timing of maximum diurnal rainfall over southeast China, Taiwan and the Luzon Island and (2) the midnight/early morning rainfall over the Yangtze River west of 110°E. This level of performance of CMCC-CM is also illustrated in the 2nd EOF mode (Supplementary Fig. S1). Together, the combination of the 1st and 2nd EOF modes explains more than 95 % of the total diurnal variability for both the observation and the model simulations. Thus, the rest of EOF modes were neglected.

To further illustrate the performance of CMCC-CM in simulating the characteristics of diurnal rainfall, we show

Fig. 4 The longitude-time evolution of observed diurnal rainfall averaged over **a** the Yangtze River regime (27°–33°N, 105°–120°E) and **b** southeast China regime (21°–25°N, 110°–118°E) extracted from long-term, 3-hourly TRMM 3B42 precipitation. The longitudinal range of the focused Yangtze River regime (105°–120°E) and southeast China regime (110°–118°E) are outlined in **a**, **b**, respectively. **c**, **d** is similar to **a**, **b**, but for the model output of CMCC-CM from historical experiment. The location of Taiwan is indicated by TW in **b**. In **c**, **d**, the maximum centers of diurnal rainfall are linked by black thick lines to help the discussions in the manuscript. The color scale and the corresponding topography averaged over the latitudinal zone of (27°–33°N) or (21°–25°N) are given in the bottom for **a**, **d**

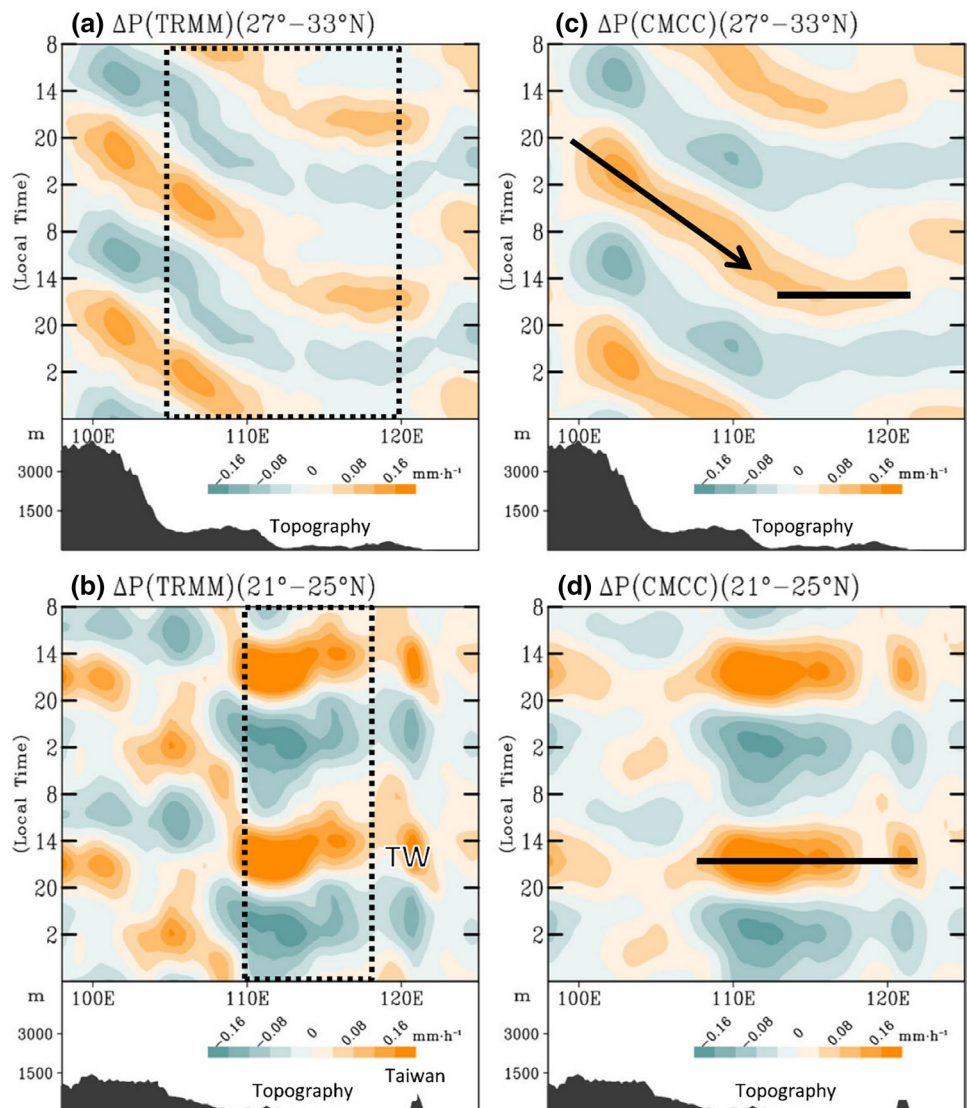


in Fig. 4 the longitude-time evolution of the observed and simulated rainfall across the Yangtze River regime (27°–33°N, 105°–120°E) and southeast China regime (21°–25°N, 110°–118°E). From the observation (Fig. 4a, b), the diurnal rainfall along the Yangtze River is characterized by an eastward propagation in the aforesaid latitudinal zones; this is in contrast to the dominant local diurnal mode over southeast China (and Taiwan around 120°E) as noted in Huang et al. (2013). In Fig. 4b, a weak propagating signal is also observed along the latitudes of 21°–25°N to the west of southeast China (i.e. the non-propagating rainfall region). All these features of diurnal rainfall were captured by CMCC-CM (Fig. 4c, d). To highlight the comparison between the observation and the CMCC-CM simulation, we removed the daily means from the observed and simulated diurnal rainfall, which is shown in Fig. 5. Compared to Fig. 4a, rainfall occurring during 14–20 LT

along the Yangtze River Valley (27°–33°N, 110°–120°E) also appears to be part of the propagating rainfall system (Fig. 5a). Other models' representation of the longitude-time evolution of diurnal rainfall across the Yangtze River and southeast China regimes is displayed in the Supplementary Figs. S2 and S3, respectively.

To more quantitatively evaluate the model performance in Figs. S2 and S3, a statistical analysis of spatial correlation (Scorr) and RMSE for each model is provided in Fig. 6. It appears that models with a better skill in terms of 1st EOF of diurnal rainfall (ref., Fig. 3), including CMCC-CM, GFDL-ESM2G, GFDL-ESM2M, MRI-CGCM3, and MRI-ESM1, also performed better in depicting the propagating regime over the Yangtze River and the non-propagating regime over the southeast China. Among all models, CMCC-CM stands out with the highest Scorr and lowest RMSE in both the propagating and non-propagating

Fig. 5 Corresponding to Fig. 4, but for the diurnal anomalies of precipitation (ΔP ; with daily mean removed). **a** ΔP (TRMM) (27°–33°N). **b** ΔP (TRMM) (21°–25°N). **c** ΔP (CMCC) (27°–33°N). **d** ΔP (CMCC) (21°–25°N)



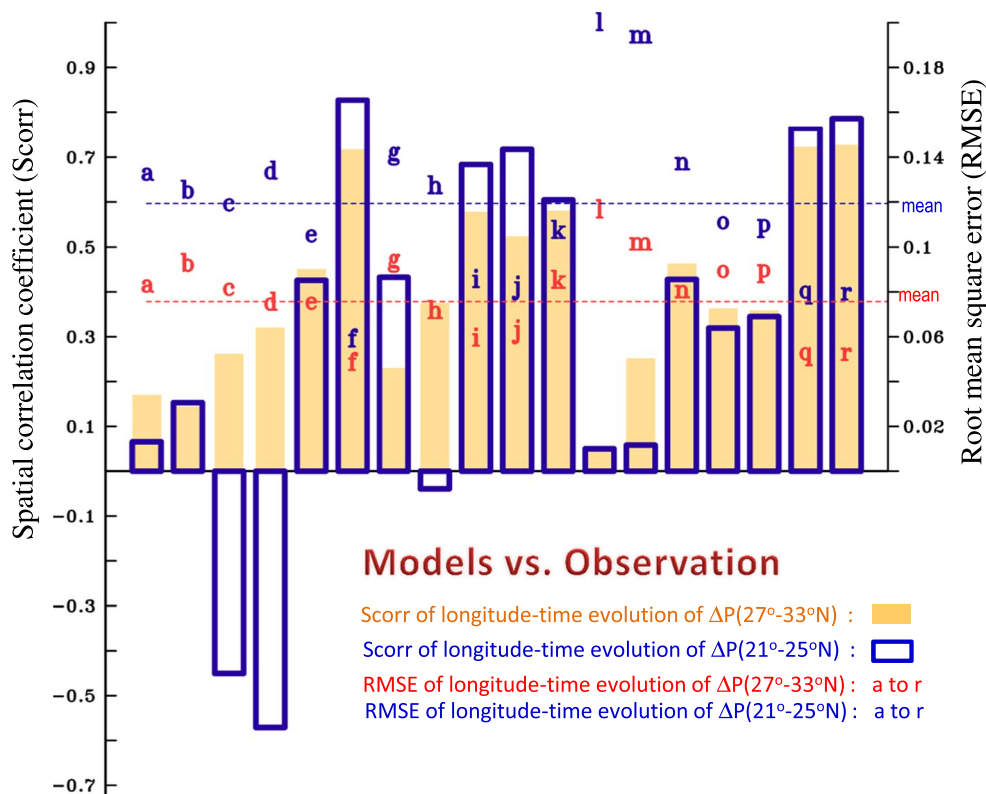


Fig. 6 Spatial correlation (Scorr) and root mean square error (RMSE) for the longitude-time evolution of ΔP ($27^{\circ}\text{--}33^{\circ}\text{N}$) (Supplementary material of Fig. S1) and ΔP ($21^{\circ}\text{--}25^{\circ}\text{N}$) (Supplemen-

tary material of Fig. S2) between 18 CMIP5 models (denoted by *a* to *r*) and TRMM observation. Full names of the models (*a* to *r*) are referred to Fig. 4

diurnal rainfall. The consistent evaluation results between Figs. 3 and 6 validate that CMCC-CM can provide a more reliable diurnal rainfall simulation.

Next, to understand the diurnal rainfall formation mechanism further, we examined the horizontal distributions of CMCC-CM's diurnal rainfall anomalies and associated convergence of column integrated moisture fluxes ($-\nabla \cdot \mathbf{Q}$)¹ based on the present climate (Fig. 7a). The role of $-\nabla \cdot \mathbf{Q}$ in contributing to the change of diurnal rainfall variation over southeast China was examined by Huang et al. (2010) through the diagnosis of water vapor budget equation.² Using observational data, Huang et al. (2010) showed that the change in diurnal rainfall over southeast China is mostly contributed by the changing $-\nabla \cdot \mathbf{Q}$ rather than by evaporation or water vapor storage alone. An earlier study by Chen (2005) also demonstrated that moisture convergence is the major factor in maintaining the change of diurnal rainfall over the East Asian summer monsoon region

(covering both southeast China and Yangtze River region). As shown in Fig. 7a, CMCC-CM was capable of capturing the diurnal variation and propagation of moisture convergence that translates into the formation of rainfall, similar to the observation (not shown). Overall, a stronger (weaker) moisture convergence corresponds to a larger (smaller) change in diurnal rainfall and this echoes the observation by Huang et al. (2013) that model's performance in depicting the moisture convergence is the key to simulating the diurnal rainfall over East Asia.

4 Future change in diurnal rainfall

4.1 CMCC-CM

Since CMCC-CM ranked the best in depicting the characteristics of diurnal rainfall over East Asia, it was selected for the following assessment of future change. Figure 7b shows the difference of CMCC-CM's rainfall and moisture convergence between the future period of 2076–2100 (under RCP4.5) and the present period of 1981–2005. Towards the end of the twenty-first century, the eastward propagating of diurnal rainfall is projected to enhance and

¹ Here, $(-\nabla \cdot \mathbf{Q}) = -\nabla \cdot \left(\int_{300\text{hPa}}^{p_0} \vec{\mathbf{V}} q dp \right)$, where \mathbf{V} denotes the horizontal wind, q is the specific humidity, and p is the pressure level.

² $P = E + (-\nabla \cdot \mathbf{Q}) + \left(-\frac{\partial W}{\partial t} \right)$, where P , E and W is the precipitation, the evaporation and the total precipitable water, respectively.

expand southward. By examining the longitude-time evolutions of the differences in precipitation and moisture convergence between the two periods, as shown in Fig. 8, the atmospheric moisture convergence following the propagating rainfall episodes will increase correspondingly. Consequently, southeast China will likely be affected by the eastward propagation diurnal rainfall episodes.

Yang and Slingo (2001) have mentioned that the rainfall over lands can propagate to adjacent oceans. Despite the limited propagating distance (Yang and Slingo 2001), it is not uncommon for the remnant of diurnal convective systems in southeast China to propagate eastward across the Taiwan Strait, which is only 180-km wide. More recently, Huang and Wang (2014) have shown that diurnal convection in Taiwan Strait can affect western Taiwan through the

interaction between a land–sea breeze-like regional circulation and the local thermally driven circulation. These previous studies lend support to the inference made here that an enhancement in the diurnal rainfall systems in southeast China can potentially impact Taiwan.

The increase in atmospheric moisture and associated convergence can be explained by the projected warming (Supplementary Fig. S4a) that would lead to an increase in water vapor evaporated from the surface (e.g., Qu et al. 2014). Also, the projected change in diurnal temperature variation (Supplementary Fig. S4b) suggests that the diurnal land–sea thermal contrast over the subtropical China will intensify under the global warming. This change in diurnal temperature can lead to an intensification of daytime sea breeze, which results in an increase of diurnal

Fig. 7 **a** The horizontal distributions of CMCC-CM’s diurnal rainfall anomalies (*shaded*) and associated convergence of column integrated moisture fluxes ($-\nabla \cdot Q$) (contoured) based on the present climate of 1981–2005 from historical experiment. **b** The difference of CMCC-CM’s rainfall and moisture convergence between the future period of 2076–2100 (under RCP4.5) and the present period of 1981–2005. In **a, b**, the vectors of moisture fluxes are added, and the *red dashed line* with symbol “X” indicates the propagation of diurnal rainfall. The *color scale* of **a, b** is given in their *right bottom*. The contour interval of **a, b** is 0.02 and 0.01 mm h^{-1} , respectively

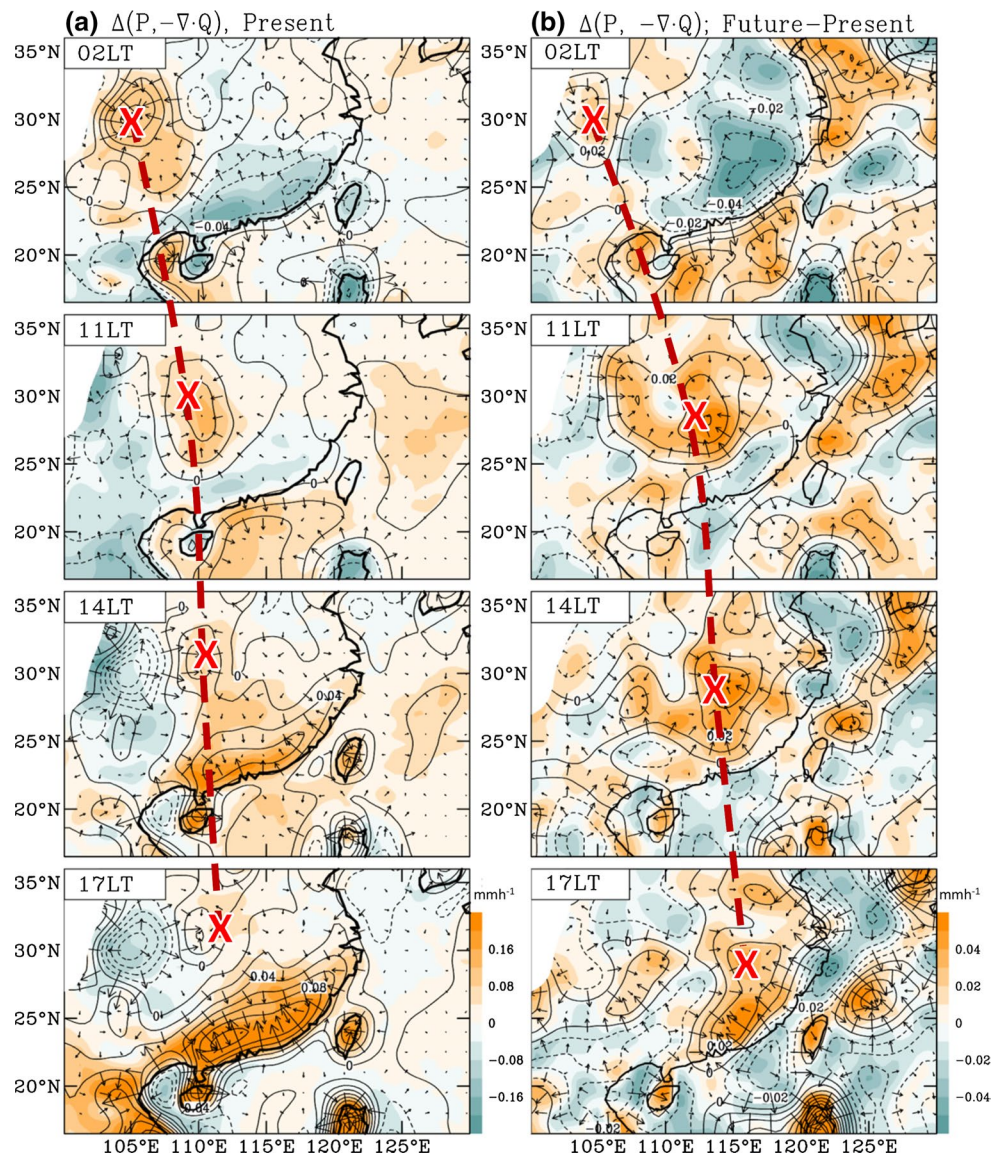
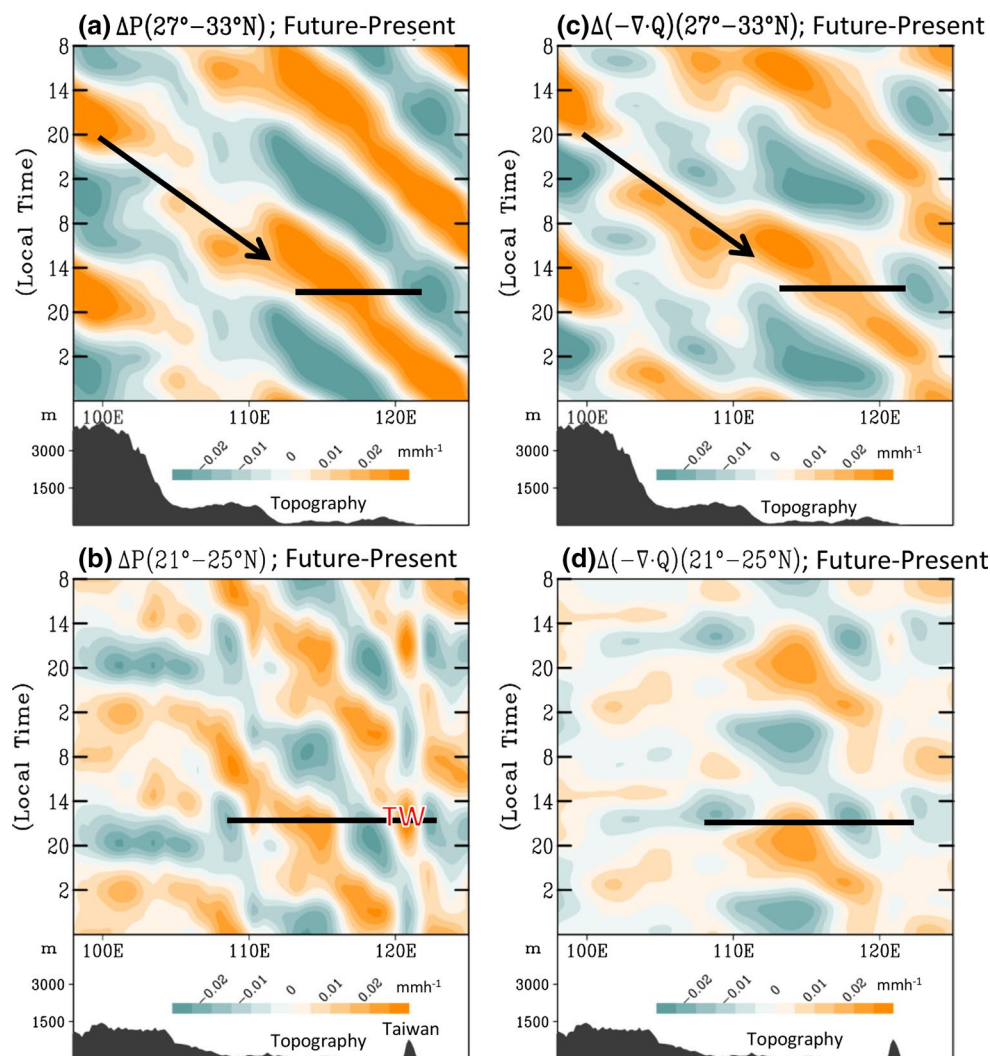


Fig. 8 Similar to Fig. 4, but for the longitude-time evolutions of the differences in precipitation between the future period of 2076–2100 (under RCP4.5) and the present period of 1981–2005 for **a** (27° – 33° N) and **b** (21° – 25° N). **c**, **d** is similar to **a**, **b**, but for the differences in moisture convergence between the two periods. To help discussions made in the paper, the black thick lines in Fig. 4c are added in **a**, **c**, while the *black thick line* in Fig. 4d is added in **b**, **d**



wind convergence in the coastal areas. Regarding the propagating feature, previous studies (e.g., Wang et al. 2004) suggested that the East Asian jet stream drives the diurnal convection initiated east of the Tibetan Plateau to propagate eastward along the Yangtze River. Examination of CMCC-CM's mean zonal wind over the subtropical China (Fig. 9a) and its future change reveals a southward shift in the region around 20° – 30° N (Fig. 9b). As shown in Fig. 9c by the vertical section of zonal wind across 105° – 115° E, the increase in westerly winds is deep (reaching 500 hPa) and this can facilitate the eastward propagation of diurnal convection, i.e. to migrate southward from central China to southeast China and Taiwan.

Earlier studies (Li et al. 2010; Sun et al. 2010; Xu et al. 2011; Zhu et al. 2012) have suggested that global warming may result in decreases of the meridional temperature

gradient (i.e. warmer north and colder south) and the jet stream over Northeast Asia. Consistent with these studies, CMCC-CM's projection of a decreased East Asian jet stream near 35° – 50° N (Fig. 9c) is associated with the decreased meridional temperature gradient north of 30° N, as inferred from Supplementary Fig. S4a. These results confirm that the projected change in upper-level atmospheric circulation plays an important role in modulating the propagation and trajectory of diurnal rainfall over East Asia; this is in agreement with what was seen in the present climate (e.g., Wang et al. 2012; Chang et al. 2015).

4.2 Other models

Even though the other CMIP5 models did not perform as well as CMCC-CM, they did provide useful information

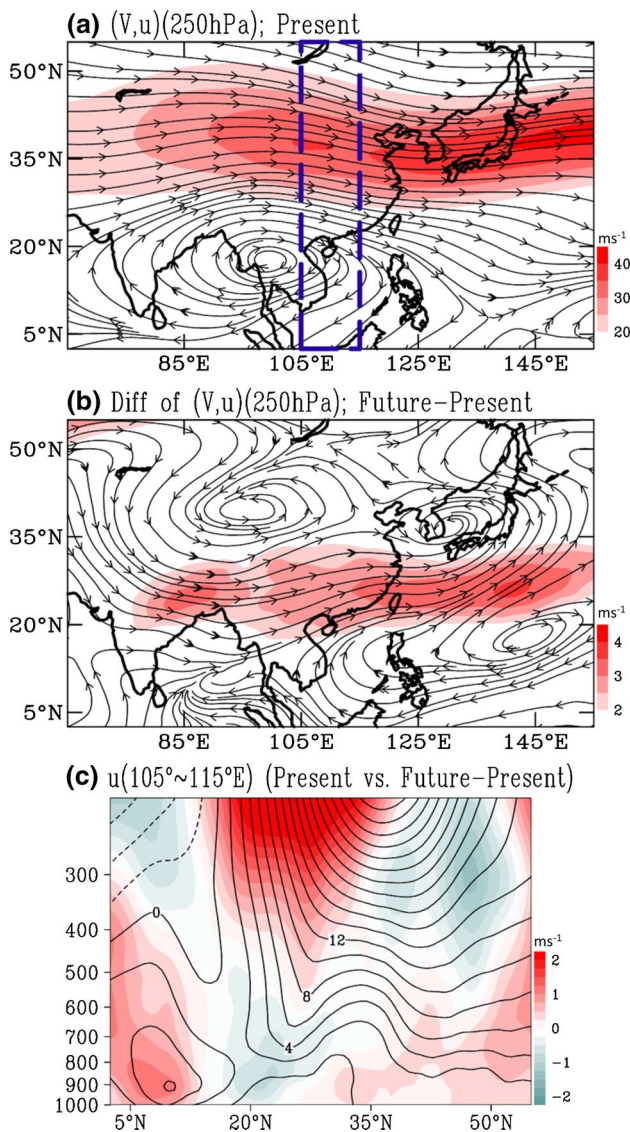


Fig. 9 **a** The horizontal distribution of CMCC-CM’s climatological mean circulation at 250 hPa, superimposed with speed of zonal wind [i.e. (V, u) (250 hPa)], based on the present climate of 1981–2005 from historical experiment. **b** The differences in (V, u) at 250 hPa between the future period of 2076–2100 (under RCP4.5) and the present period of 1981–2005. **c** The vertical cross-section of u averaged over $(105^{\circ}\text{--}115^{\circ}\text{E})$ for the present climate (contoured) superimposed with its related differences in u between future and present (shaded). The domain of $(105^{\circ}\text{--}115^{\circ}\text{E})$ is outlined in **a**. The color scale of **a–c** is given in their right bottom, and the contour interval of **c** is 2 ms^{-1}

about the projection of large-scale circulation patterns and associated diurnal rainfall. Here, we examined the vertical section of zonal wind across $105^{\circ}\text{--}115^{\circ}\text{E}$ (Supplementary Fig. S5) and the longitude-time evolution of diurnal rainfall

(Supplementary Figs. S6, S7) projected by the individual models. Except for CMCC-CM, four models (GFDL-ESM2G, GFDL-ESM2M, MRI-CGCM3, and MRI-ESM1) that show a better skill in Figs. 3 and 6 also projected an increase in westerly wind over $20^{\circ}\text{--}35^{\circ}\text{N}$. Corresponding to this circulation change, these four models projected an increase in the eastward propagating rainfall over East Asia; this can be seen in the Supplementary Figs. S6 and S7. The consistent projections of these four models lend support to the CMCC-CM’s projected change in diurnal rainfall and associated dynamical mechanisms. Together, the ensemble projections of the diurnal rainfall evolution and associated dynamical mechanisms from these five better-skill models are displayed in Figs. 10a and 11a–c, respectively.

By comparison, most other models with a poor skill in the diurnal rainfall only depicted the non-propagating feature (Supplementary Figs. S2, S3). For these models, most of the projections of large-scale circulation show that the upper-level westerly wind over $(105^{\circ}\text{--}115^{\circ}\text{E}, 20^{\circ}\text{--}35^{\circ}\text{N})$ will weaken in the future (Supplementary Fig. S5), while the projected diurnal rainfall will still be dominated by local convection (Supplementary Figs. S6, S7). Regardless, these poor-skill models showed a corresponding relationship between the projected changes in the eastward propagation of diurnal rainfall and the large-scale circulation (i.e. a weaker westerly jet with a weaker eastward propagation); this is shown in Figs. 10b and 11d–f.

5 Conclusion

The capability of 18 CMIP5 models in simulating the characteristics of diurnal rainfall over the Yangtze River and southeast China were evaluated using outputs from the historical experiment. Results show that one particularly correct model, CMCC-CM, was capable of depicting both the correct timing of propagating diurnal rainfall over the Yangtze River and the non-propagating diurnal rainfall over southeast China. Diagnostic analyses further indicated that the performance of CMCC-CM in depicting the diurnal rainfall over East Asia is related to its simulations of moisture convergence, which is a major driver of diurnal rainfall in the region. Based upon the future changes of rainfall and moisture convergence simulated by CMCC-CM (under RCP4.5), the eastward propagation of diurnal rainfall will likely enhance and expand southward towards the end of the twenty-first century. This tendency means that southeast China and Taiwan will increasingly experience the eastward-propagating episodes of diurnal rainfall.

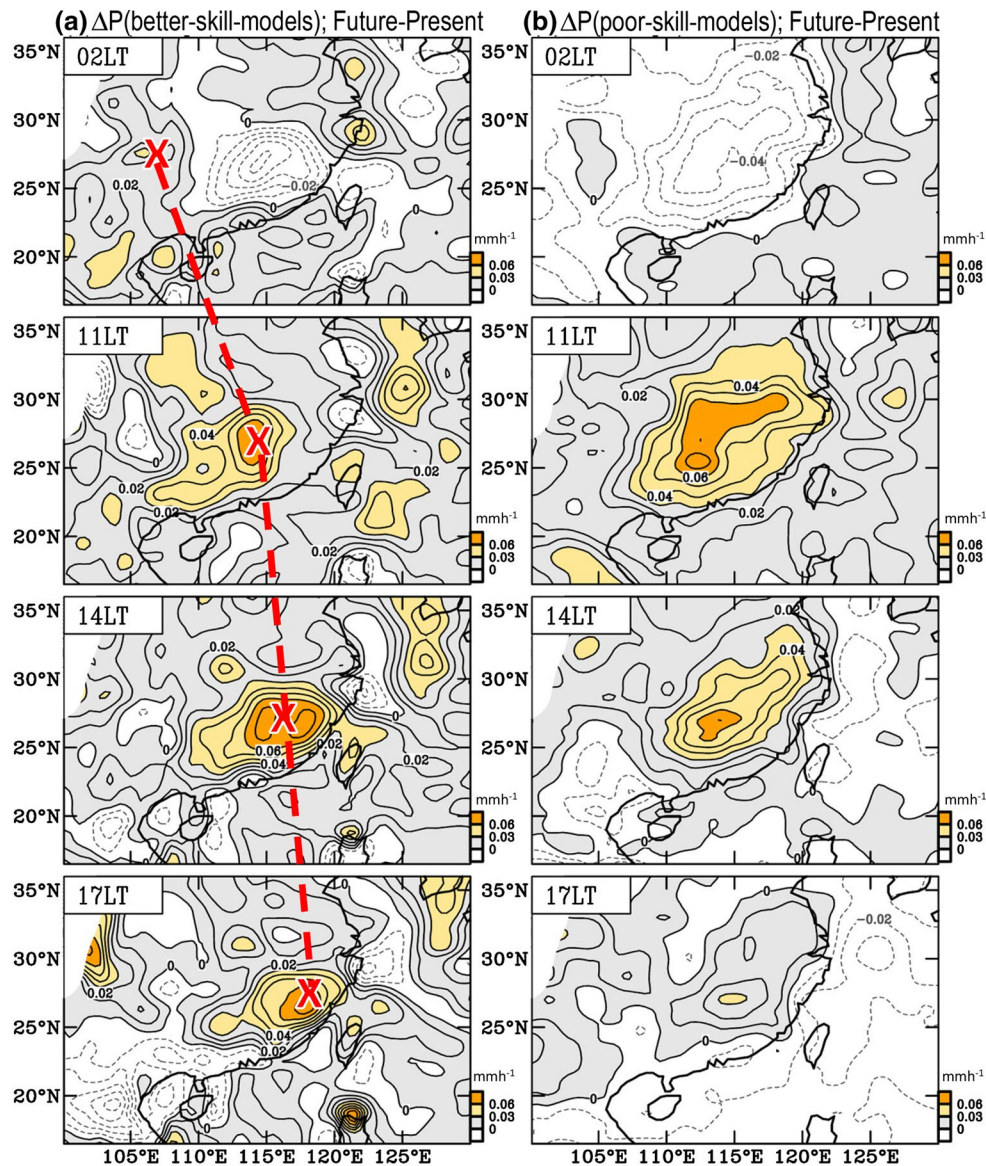


Fig. 10 **a** The difference of ensemble mean of rainfall between the future period of 2076–2100 (under RCP4.5) and the present period of 1981–2005 for the five better-skill-models (including CMCC-CM, GFDL-ESM2G, GFDL-ESM2M, MRI-CGCM3, and MRI-ESM1, which shows better skill in Figs. 3, 6). **b** is similar to **a**, but

for the ensemble mean of poor-skill-models (rest models). In **a**, the red dashed line with symbol “X” indicates the propagation of diurnal rainfall. The color scale of **a**, **b** is given in their right bottom. The contour interval of **a**, **b** is 0.01 mm h^{-1}

Possible causes of the intensification of diurnal rainfall variation and eastward propagating feature were discussed. The projected intensification of diurnal rainfall is attributed to the intensification of diurnal land–sea thermal contrast over eastern China under the warming climate, in which stronger daytime sea breeze coupled with more water vapor evaporated from the surface promotes moisture convergence over land. These changes in atmospheric thermodynamic conditions support the projected intensification of

diurnal rainfall. Meanwhile, the intensification of upper-level westerly wind revealed over 20° – 30° N will shift (or expand) the eastward propagation of diurnal rainfall southward, likely into the non-propagating regime in southeast China and Taiwan. Notably, except for CMCC-CM, four other models (GFDL-ESM2G, GFDL-ESM2M, MRI-CGCM3, and MRI-ESM1) also projected the increase in westerly jet over 20° – 35° N and the enhancement in the eastward propagating rainfall over East Asia. The consistent

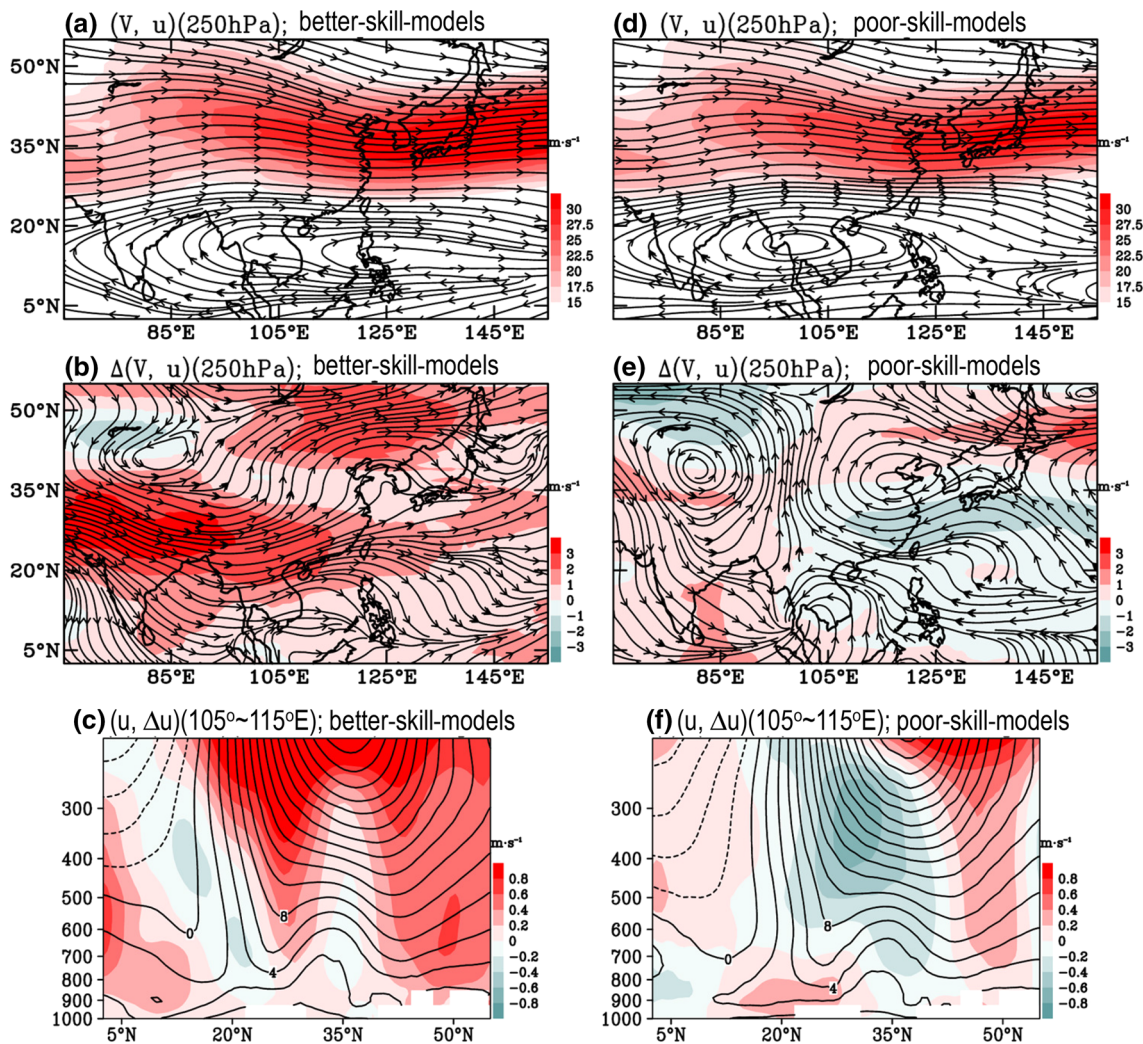


Fig. 11 Similar to Fig. 9, but for the ensemble mean of **a–c** better-skill-models (including CMCC-CM, GFDL-ESM2G, GFDL-ESM2M, MRI-CGCM3, and MRI-ESM1) and **d–f** poor-skill-models

(rest models). The identification of better-skill-models and poor-skill-models are based on the results of Figs. 3 and 6 (see related discussion in Sect. 4)

projections of these models lend support to the suggested mechanism from which future diurnal rainfall will evolve in response to the large-scale circulation changes. Future work should focus on understanding coupled models’ performance of the large-scale rainfall and convective rainfall separately, and associated maintenance mechanisms.

Acknowledgments The authors thank anonymous reviewers for their comments and suggestions which greatly improved the manuscript. We thank the climate modeling groups (listed in Table 1 of this paper) for producing and making available their model output, and Mr. Kuan-Chieh Chen for assisting data downloading processes. This research was supported by the Ministry of Science and Technology of Taiwan under MOST 104-2111-M-003-001, MOST 105-2119-M-003-002 and MOST 105-2625-M-003-002, as well as Grant MOTC-CWB-105-M-09 and MOTC-CWB-101-M-15 of the Central Weather Bureau.

Open Access This article is distributed under the terms of the Creative Commons Attribution 4.0 International License (<http://creativecommons.org/licenses/by/4.0/>), which permits unrestricted use, distribution, and reproduction in any medium, provided you give appropriate credit to the original author(s) and the source, provide a link to the Creative Commons license, and indicate if changes were made.

References

Arakawa O, Kitoh A (2005) Rainfall diurnal variation over the Indonesian maritime continent simulated by 20 km-mesh GCM. SOLA 1:109–112
 Asai T, Ke S, Kodama Y (1998) Diurnal variability of cloudiness over East Asia and the western Pacific Ocean as revealed by GMS during the warm season. J Meteorol Soc Jpn 76:675–684

- Bacmeister JT, Wehner M, Neale RB, Gettelman A, Hannay C, Lauritzen P, Caron J (2013) Exploratory high-resolution climate simulations using the Community Atmosphere Model (CAM). *J Clim* 27:3073–3099
- Betts AK, Jakob C (2002) Evaluation of the diurnal cycle of precipitation, surface thermodynamics, and surface fluxes in the ECMWF model using LBA data. *J Geophys Res* 107:8045
- Bi D et al (2013) The ACCESS coupled model: description, control climate and preliminary validation. *Aust Meteorol Oceanogr* 42:63–64
- Chang FR, Huang WR, Wang CC (2015) The effects of long-term climate change on eastward propagating rainfall events over the yangtze river valley: example of may 2009. *Atmos Sci* 43:265–284 (in Chinese with an English abstract)
- Chen TC (2005) Variation of the Asian monsoon water vapor budget: interaction with the global-scale modes. In: Wang B (ed) *The Asian monsoon*. Springer, Berlin, pp 417–458
- Chen G, Sha W, Iwasaki T (2009) Diurnal variation of precipitation over southeastern China: spatial distribution and its seasonality. *J Geophys Res* 114:D13103
- Collier JC, Bowman KP (2004) Diurnal cycle of tropical precipitation in a general circulation model. *J Geophys Res* 109:D17105
- Dai A (2006) Precipitation characteristics in eighteen coupled climate models. *J Clim* 19:4605–4630
- Dai A, Trenberth KE (2004) The diurnal cycle and its depiction in the community climate system model. *J Clim* 17:930–951
- Dirmeyer PA et al (2011) Simulating the diurnal cycle of rainfall in global climate models: resolution versus parameterization. *Clim Dyn* 39:399–418
- Donner LJ et al (2011) The dynamical core, physical parameterizations, and basic simulation characteristics of the atmospheric component AM3 of the GFDL global coupled model CM3. *J Clim* 24:3484–3519
- Dufresne JL et al (2013) Climate change projections using the IPSL-CM5 Earth System Model: from CMIP3 to CMIP5. *Clim Dyn* 40:2123–2165
- Hara M, Yoshikane T, Takahashi HG, Kimura F, Noda A, Tokioka T (2009) Assessment of the diurnal cycle of precipitation over the Maritime Continent simulated by a 20 km mesh GCM using TRMM PR data. *J Meteorol Soc Jpn* 87:413–424
- Hirose M, Nakamura K (2005) Spatial and diurnal variation of precipitation systems over Asia observed by the TRMM Precipitation Radar. *J Geophys Res* 110:D05106
- Hong Y, Hsu KL, Sorooshian S, Gao X (2005) Improved representation of diurnal variability of rainfall retrieved from the tropical rainfall measurement mission microwave imager adjusted Precipitation estimation from Remotely Sensed Information Using Artificial Neural Networks (PERSIANN) system. *J Geophys Res* 110:D06102
- Hsu HH, Zhou T, Matsumoto J (2014) East Asian, Indochina and western North Pacific summer monsoon—an update. *Asia Pac J Atmos Sci* 50:45–68
- Huang WR, Chan JCL (2012) Seasonal variation of diurnal and semi-diurnal variation of rainfall over Southeast China. *Clim Dyn* 39:1913–1927
- Huang WR, Chen KC (2015) Trends in pre-summer frontal and diurnal rainfall activities during 1982–2012 over Taiwan and Southeast China: characteristics and possible causes. *Int J Climatol* 35:2608–2619
- Huang WR, Wang SY (2014) Impact of land–sea breezes at different scales on the diurnal rainfall in Taiwan. *Clim Dyn* 43:1951–1963
- Huang WR, Chan JCL, Wang SY (2010) A planetary-scale land–sea breeze circulation in East Asia and the western North Pacific. *Q J R Meteorol Soc* 136:1543–1553
- Huang WR, Chan JCL, Au-Yeung AYM (2013) Regional climate simulations of summer diurnal rainfall variations over East Asia and Southeast China. *Clim Dyn* 40:1625–1642
- Ji D et al (2014) Description and basic evaluation of Beijing Normal University Earth System Model (BNU-ESM) version 1. *Geosci Model Dev* 7:2039–2064
- Kikuchi K, Wang B (2008) Diurnal precipitation regimes in the global tropics. *J Clim* 21:2680–2696
- Lee MI et al (2007) Sensitivity to horizontal resolution in the AGCM simulations of warm season diurnal cycle of precipitation over the United States and Northern Mexico. *Clim Dyn* 20:1862–1881
- Li J, Yu R, Zhou T (2008) Seasonal variation of the diurnal cycle of rainfall in southern contiguous China. *J Clim* 21:6036–6043
- Li J, Wu Z, Jiang Z, He J (2010) Can global warming strengthen the East Asian summer monsoon? *J Clim* 23:6696–6705
- Li J, Yu R, Yuan W, Chen H, Sun W, Zhang Y (2015) Precipitation over East Asia simulated by NCAR CAM5 at different horizontal resolutions. *J Adv Model Earth Syst* 7:774–790
- Lin X, Randall DA, Fowler LD (2000) Diurnal variability of the hydrologic cycle and radiative fluxes: comparisons between observations and a GCM. *J Clim* 13:4159–4179
- Madec G, Delecluse P, Imbard M, Levy C (1998) OPA8.1 Ocean general circulation model reference manual. Institut Pierre-Simon Laplace (IPSL) technical report, No 11
- Nesbitt SW, Zipser EJ (2003) The diurnal cycle of rainfall and convective intensity according to three years of TRMM measurements. *J Clim* 16:1456–1475
- Nordeng TE (1994) Extended versions of the convective parameterization scheme at ECMWF and their impact on the mean and transient activity of the model in the tropics. ECMWF Technical Memorandum 206
- Oki T, Musiaka K (1994) Seasonal change of the diurnal cycle of precipitation over Japan and Malaysia. *J Appl Meteorol* 33:1445–1463
- Ploshay JJ, Lau NC (2010) Simulation of the diurnal cycle in tropical rainfall and circulation during boreal summer with a high-resolution GCM. *Mon Weather Rev* 138:3434–3453
- Qu X, Huang G, Zhou W (2014) Consistent responses of East Asian summer mean rainfall to global warming in CMIP5 simulations. *Theor Appl Climatol* 117:123–131
- Rienecker MM et al (2011) MERRA: NASA’s modern-era retrospective analysis for research and applications. *J Clim* 24:3624–3648
- Roeckner E et al (2006) Sensitivity of simulated climate to horizontal and vertical resolution in the ECHAM5 atmosphere model. *J Clim* 19:3771–3790
- Sato T, Miura H, Satoh M, Takayabu YN, Wang YQ (2009) Diurnal cycle of precipitation in the tropics simulated in a global cloud-resolving model. *J Clim* 22:4809–4826
- Scoccimarro E et al (2011) Effects of tropical cyclones on ocean heat transport in a high resolution coupled general circulation model. *J Clim* 24:4368–4384
- Simpson JS, Kummerow C, Tao WK, Adler RF (1996) On the tropical rainfall measuring mission (TRMM). *Meteorol Atmos Phys* 60:19–36
- Slingo A, Hodges KI, Robinson GJ (2004) Simulation of the diurnal cycle in a climate model and its evaluation using data from Meteosat 7. *Q J R Meteorol Soc* 130:1449–1467
- Sorooshian S, Gao X, Hsu K, Maddox RA, Hong Y, Gupta HV, Imam B (2002) Diurnal variability of tropical rainfall retrieved from combined GOES and TRMM satellite information. *J Clim* 15:983–1001
- Sun Y, Ding Y, Dai A (2010) Changing links between South Asian summer monsoon circulation and tropospheric land–sea thermal contrasts under a warming scenario. *Geophys Res Lett* 37:L02704

- Taylor KE, Stouffer RJ, Meehl GA (2012) An overview of CMIP5 and the experiment design. *Bull Am Meteorol Soc* 93:485–498
- Tiedtke M (1989) A comprehensive mass flux scheme for cumulus parameterization in large-scale models. *Mon Weather Rev* 117:1779–1800
- Volodire A et al (2013) The CNRM-CM5.1 global climate model: description and basic evaluation. *Clim Dyn* 40:2091–2121
- Volodin EM, Dianskii NA, Gusev AV (2010) Simulating present-day climate with the INMCM4.0 coupled model of the atmospheric and oceanic general circulations. *Izvestiya Atmos Ocean Phys* 46:414–431
- Wallace JM (1975) Diurnal variations in precipitation and thunderstorm frequency over the conterminous United States. *Mon Weather Rev* 103:406–419
- Wang CC, Chen GTJ, Carbone RE (2004) A climatology of warm-season cloud patterns over east Asia based on GMS infrared brightness temperature observations. *Mon Weather Rev* 132:1606–1629
- Wang CC, Chen GTJ, Carbone RE (2005) Variability of warm-season cloud episodes over east Asia based on GMS infrared brightness temperature observations. *Mon Weather Rev* 133:1478–1500
- Wang Y, Zhou L, Hamilton K (2007) Effect of convective entrainment/detrainment on the simulation of the tropical precipitation diurnal cycle. *Mon Weather Rev* 135:567–585
- Wang CC, Chen GTJ, Huang HL, Carbone RE, Chang SW (2012) Synoptic conditions associated with propagating and nonpropagating cloud/rainfall episodes during the warm season over the East Asian continent. *Mon Weather Rev* 140:721–747
- Watanabe S et al (2011) MIROC-ESM 2010: model description and basic results of CMIP5-20c3m experiments. *Geosci Model Dev* 4:845–872
- Xin X, Wu T, Zhang J (2013) Introduction of CMIP5 experiments carried out with the climate system models of Beijing Climate Center. *Adv Clim Change Res* 4:41–49
- Xu K, Zhu C, He J (2011) Impact of the surface air temperature warming around Lake Baikal on trend of summer precipitation in north China in the past 50 years. *Plateau Meteorol* 30:309–317 (in Chinese)
- Yang GY, Slingo J (2001) The diurnal cycle in the tropics. *Mon Weather Rev* 129:784–801
- Yu R, Xu Y, Zhou T, Li J (2007a) Relation between rainfall duration and diurnal variation in the warm season precipitation over central eastern China. *Geophys Res Lett* 34:L13703
- Yu R, Zhou T, Xiong A, Zhu Y, Li J (2007b) Diurnal variations of summer precipitation over contiguous China. *Geophys Res Lett* 34:L01704
- Yu R, Li J, Chen H (2009) Diurnal variation of surface wind over central eastern China. *Clim Dyn* 33:1089–1097
- Yuan W (2013) Diurnal cycles of precipitation over subtropical China in IPCC AR5 AMIP simulations. *Adv Atmos Sci* 30:1679–1694
- Yuan W, Yu R, Zhang M, Lin W, Chen H, Li J (2012) Regimes of diurnal variation of summer rainfall over subtropical East Asia. *J Clim* 25:3307–3320
- Yuan W, Yu R, Zhang M, Lin W, Li J, Fu Y (2013) Diurnal cycle of summer precipitation over subtropical East Asia in CAM5. *J Clim* 26:3159–3172
- Yukimoto S et al (2012) A new global climate model of Meteorological Research Institute: MRI-CGCM3—model description and basic performance. *J Meteorol Soc Jpn* 90A:23–64
- Zhang GJ (2003) Roles of tropospheric and boundary layer forcing in the diurnal cycle of convection in the U.S. southern great plains. *Geophys Res Lett* 30:2281
- Zhao Z, Leung LR, Qian Y (2005) Characteristics of diurnal variations of precipitation in China for the recent years. CLIVAR Exchanges, No. 3, International CLIVAR Project Office, Southampton, United Kingdom, pp 24–26
- Zhou T, Yu R, Chen H, Dai A, Pan Y (2008) Summer precipitation frequency, intensity, and diurnal cycle over China: a comparison of satellite data with rain gauge observations. *J Clim* 21:3997–4010
- Zhu C, Wang B, Qian W, Zhang B (2012) Recent weakening of northern East Asian summer monsoon: a possible response to global warming. *Geophys Res Lett* 39:L09701